

Orbital-scale competition of biogenic carbonate and opal production and its implication on carbon cycle at Del Caño Rise in the Indian sector of the Southern Ocean

Hyuk Choi ^a, Xavier Crosta ^b, Isabelle Billy ^b, Tomohisa Irino ^c, Sangbeom Ha ^d, Hiroyuki Takata ^{a,f}, Boo-Keun Khim ^{e,*}

^a School of Earth Environmental Systems, Pusan National University, Busan 46241, Republic of Korea

^b Université de Bordeaux, CNRS, Bordeaux INP, UMR 5805 EPOC, 33615 Pessac Cedex, France

^c Faculty of Environmental Earth Science, Hokkaido University, Sapporo 060-0810, Japan

^d Division of Glacial and Earth Sciences, Korea Polar Research Institute, Incheon 21990, Republic of Korea

^e Department of Oceanography and Marine Research Institute, Pusan National University, Busan 46241, Republic of Korea

^f Faculty of Dinosaur Paleontology, Fukui Prefecture University, Eiheiji 910-1195, Japan

ARTICLE INFO

Editor: M Elliott

Keywords:

Phytoplankton production
Ocean front
Ventilation
Carbon cycle
Southern Ocean

ABSTRACT

Geochemical properties measured in core MD19-3575CQ, collected from the Del Caño Rise within the Subantarctic Zone in the Indian sector of the Southern Ocean, provide evidence of orbital-scale changes over eccentricity, obliquity, and precession cycles in phytoplankton productivity and its influence on the organic matter burial over the last 235 kyr. CaCO_3 and biogenic opal contents varied oppositely with high CaCO_3 and low biogenic opal contents during the interglacial periods and *vice versa* during the glacial periods. During the glacial periods, the biogenic opal production by diatoms increased as a result of more silica supply when the Subantarctic Front shifted northward across the Del Caño Rise. In addition, Fe-bearing dust and remobilized sediments likely enhanced diatom productivity. In contrast, biogenic carbonate production by coccolithophores and foraminifera was reduced during the glacial periods because of cold ocean temperature and competition for nutrients between coccolithophores and diatoms. More organic carbon was buried at the core site during the glacial periods than during the interglacial periods, probably in relation to a greater export efficiency by diatoms relative to coccolithophores as well as a better preservation of the organic matter when the Circumpolar Deep Water was less ventilated during the glacial periods.

1. Introduction

The surface waters of the Southern Ocean are structured by the Antarctic Circumpolar Current (ACC), a strong eastward flow that divides the region into distinct zones with contrasting physical and chemical properties (Orsi et al., 1995; Rintoul et al., 2001). Major oceanic fronts, such as the Subantarctic Front (SAF) and Antarctic Polar Front (APF), further delineate these surface water masses. In the Antarctic Divergence Zone (ADZ), wind-driven surface water divergence induces the upwelling of Circumpolar Deep Water (CDW). The upwelled CDW supplies nutrients (*i.e.*, silica and nitrate) to the surface waters, supporting primary productivity. This water is then transported both northward and southward within the surface layer by Ekman transport,

and part of it contributes to the formation of Antarctic Bottom Water (AABW) along the Antarctic continental margin. Both overturning cells provide a direct connection between the atmosphere and the deep ocean and play an important role in exchanging CO_2 between the atmosphere and ocean (Rintoul and Garabato, 2013). In addition, the biological carbon pump (BCP) in the Southern Ocean actively modulate the CO_2 fluxes at the atmosphere-ocean interface (Sigman and Boyle, 2000). The BCP refers to the process by which phytoplankton converts atmospheric CO_2 through photosynthesis into organic carbon, which sinks to the deep sea and seafloor, thereby effectively removing atmospheric CO_2 for hundreds to thousands of years. Diatoms, unicellular photosynthetic algae encapsulated with siliceous test termed frustule, are the most important primary producers in the Antarctic Zone (AZ), south of APF of

* Corresponding author.

E-mail address: bkkhim@pusan.ac.kr (B.-K. Khim).

the Southern Ocean (e.g., Rigual-Hernández et al., 2015). They uptake CO₂ through the photosynthesis and export the organic matter efficiently toward the deep sea (Boyd and Newton, 1999). On the other hand, coccolithophores dominate surface water productivity in the Subantarctic Zone (SAZ), north of the SAF (e.g., Balch et al., 2011; Rigual-Hernández et al., 2020). The carbonate counter pump (CCP) refers to the process by which calcifying organisms such as coccolithophores and foraminifera release CO₂ into seawater during the formation of their calcium carbonate shells, thereby counteracting CO₂ uptake by photosynthesis. While coccolithophores consume CO₂ through the photosynthesis, both coccolithophores and foraminifera release CO₂ during the elevated carbonate production, thereby enhancing the effect of the CCP (Duchamp-Alphonse et al., 2018). The balance between siliceous and carbonate production in the Southern Ocean, therefore, has greatly impacted on past atmospheric CO₂ concentrations (Sigman and Boyle, 2000).

The surface waters of the AZ has high dissolved silica (DSi) concentration (50–15 μM) that supports high diatom primary production, while lower DSi concentration (<10 μM) and low diatom production are observed in the north of APF (Fig. 2). Unlike diatoms, coccolithophores are not limited by DSi concentration, and seawater temperature is the primary factor controlling their distribution in the Southern Ocean (Holligan et al., 2010; Saavedra-Pellitero et al., 2014). In this vein, coccolithophores dominate phytoplankton productivity in the warmer and DSi poor Subantarctic Zone (SAZ). However, this pattern was different during the glacial periods, with a decrease of diatom productivity south of the APF and an increase north of the APF (Charles et al., 1991; Nair et al., 2020; Shukla et al., 2023). At the same time, opposite to the diatom productivity, coccolithophore productivity decreased north of the APF during the glacial periods (Manoj and Thamban, 2015; Choudhari et al., 2023). In other words, changes in dominant phytoplankton communities during the glacial-interglacial cycles have played a critical role on the ocean's carbon storage capacity through the BCP and CCP, essentially north of the APF (Sigman and Boyle, 2000).

Orbital-scale variations, particularly precession (~23 kyr) and eccentricity (~100 kyr), modulate primary productivity by driving changes in oceanic fronts, nutrient availability, upwelling intensity, and sea ice extent (e.g., Crosta et al., 2007). These mechanisms collectively regulate biogenic carbonate and opal production across various oceanic regions. However, productivity changes at glacial-interglacial cycles in the Southern Ocean are mostly reported from the Atlantic and Pacific sectors. In the Pacific sector, glacial productivity changes were mainly influenced by oceanic front migrations, but their impact was often regionally limited due to local bathymetry (Chase et al., 2003; Studer et al., 2015). In the Atlantic sector, although similar mechanisms operated between the glacial and interglacial periods, productivity was further enhanced by the substantial aeolian input from the Patagonia during the glacial periods (Martínez-García et al., 2014; Jaccard et al., 2013). In the Indian sector, orbital-scale productivity changes have been primarily attributed to shift in oceanic fronts (Manoj and Thamban, 2015; Shukla et al., 2023). However, the previous studies remain limited in scope, often relying on single proxies and covering shorter timescales. For example, Manoj and Thamban (2015) reconstructed paleoproductivity changes using diatom-coccolithophore multiproxy approach, but their record spans only ~95 ka, while Shukla et al. (2023) focused on high-resolution diatom data to investigate orbital-scale variability. Despite these efforts, comprehensive analyses integrating multiple productivity proxies over the long timescales in this region are still lacking.

This study investigates orbital-scale changes in biogenic carbonate and siliceous productivity over the past 235,000 years using sediment core MD19-3575CQ from the Del Caño Rise, located within the SAZ in the Indian sector of the Southern Ocean. Unlike previous studies in this region, our study utilizes both biogenic carbonate and opal proxies to reconstruct long-term paleoproductivity changes. With this approach, we aim to clarify the relationships between surface water productivity,

ocean circulation, and the ocean's carbon storage capacity in the SAZ, in relation to orbital-scale glacial-interglacial climate cycles.

2. Study area

The Del Caño Rise is located in the Indian sector of the Southern Ocean (Fig. 1). It lies within the eastward flowing ACC between the Subtropical Front (STF) to the north and the APF to the south (Fig. 1). This region consists of an elevated topography, with a water depth of approximately 2400 m, that diverts the SAF to the south. The SAF is a thermohaline hydrological front that separates the nutrient-rich surface waters of the AZ from the nutrient-poor surface waters of the SAZ (Bowie et al., 2011).

CDW upwells in the ADZ, located in the south of the AZ, supplying a large amount of nutrients, including nitrate and silicate, to the surface (Rintoul and Garabato, 2013). The nutrients supplied to the surface are transported equatorward by the Ekman component of the ACC. They are also utilized and depleted by primary production in the surface layer, resulting in a decrease in nutrient concentration as they cross the oceanic fronts (Fig. 2; Tréguer, 2014). The interaction of the ACC with the bathymetric highs also promotes an active eddy field and a regional upwelling of deep nutrients (Tamsitt et al., 2017). Both processes support a higher-than-usual regional phytoplankton productivity.

The shallow water depth of the Del Caño Rise, well above the calcite lysocline depth observed at ~3400 m depth at 45°S (Howard and Prell, 1994), favors the calcareous sediment deposition and preservation. In particular, during the interglacial periods, the influence of well-ventilated North Atlantic Deep Water (NADW), characterized by a high concentration of carbonate ions [CO₃²⁻] and a state of calcite supersaturation (González-Dávila et al., 2011), may have further enhanced carbonate preservation in the study area. As a result, surface sediments in the Del Caño Rise exhibit high carbonate contents of up to ~75 % (Choudhari et al., 2023). In contrast, carbonate preservation may have been less efficient during the glacial periods due to the reduced influence of NADW and increased contribution from southern-sourced deep waters such as the CDW and AABW, which are relatively undersaturated in [CO₃²⁻], thereby enhancing carbonate dissolution (Gottschalk et al., 2018). Nevertheless, the shallow water depth of the Del Caño Rise likely limited the extent of carbonate dissolution even during the glacial periods, thereby supporting continuous carbonate preservation. Consequently, the geochemical signals in the study area retain high stratigraphic resolution and reliability across the glacial-interglacial cycles.

3. Materials and methods

The 8.09 m long sediment core MD19-3575CQ (IGSN IEFRA09CX) was retrieved from the Del Caño Rise (46°02'49"S, 44°22'13"E; water depth of 2410 m) during the MD218 CROTALE expedition (<https://doi.org/10.17600/18000886>) aboard the R/V Marion Dufresne in 2019 (Fig. 1). GEOTEK Multi Sensor Core Logger (MSCL) was utilized to measure the preliminary sediment properties such as sediment colors (L*, a*, and b*) and magnetic susceptibility (MS) at 1 cm interval after the visual observation for lithologic description at University of Bordeaux (France).

3.1. Core chronology

The chronology of core MD19-3575CQ was based on two complementary approaches: Accelerator Mass Spectrometry (AMS) ¹⁴C dating and stable isotope measurement of planktonic foraminifera. Four AMS ¹⁴C datings of planktonic foraminifera (*Neogloboquadrina pachyderma* and *Globigerina bulloides*) in the upper part (5 cm, 20 cm, 80 cm, and 155 cm) of the core were conducted at Beta Analytic (USA). The measured ¹⁴C ages were converted to the calendar years (cal yr BP) using CALIB 8.20 (Stuiver and Reimer, 1993) considering the reservoir effect of the

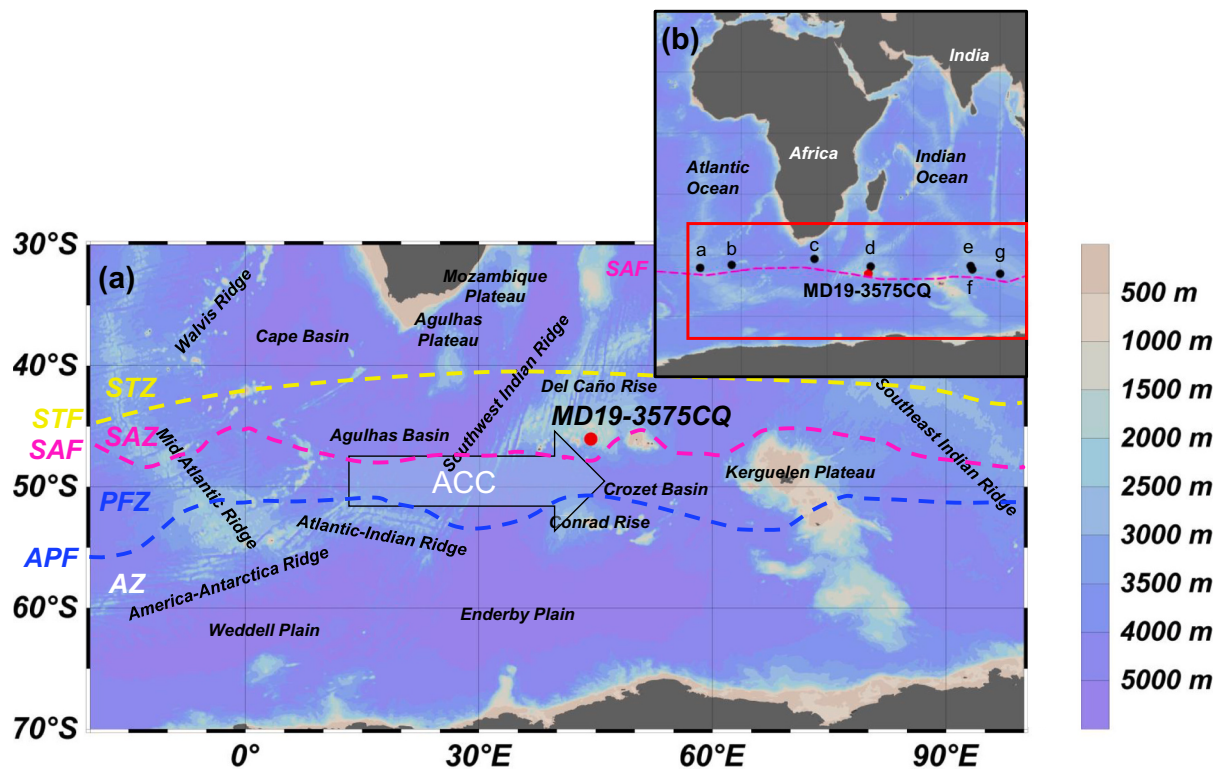


Fig. 1. (a) Map showing the core location (MD19-3575CQ), the oceanic fronts (Antarctic Polar Front: APF, Subantarctic Front: SAF and Subtropical Front: STF) and the frontal zones (Antarctic Polar Frontal zone: APZ, Subantarctic Frontal zone: SAZ and Subtropical Frontal Zone: STZ) in the southwestern Indian sector of the Southern Ocean. The geographic location of core MD19-3575CQ belongs to the Subantarctic Zone in the Southern Ocean (modified after Orsi et al., 1995). ACC: Antarctic Circumpolar Current. (b) Map showing the core locations including MD19-3575CQ (this study) with the reported cores: (a) PS2498-1 (Anderson et al., 2014), (b) V22-108 (Charles et al., 1991), (c) MD02-2588 (Romero et al., 2015), (d) SK200/22a (Manoj and Thamban, 2015), (e) RC11-120 (Charles et al., 1991), (f) MD11-3357 (Thöle et al., 2019), and (g) MD88-769 (Rosenthal et al., 1995).

study area in the MARINE 20 database (Heaton et al., 2020). An AMS ^{14}C age ($>43,500$ yr BP) at 155 cm depth was excluded in the reconstruction of age model because it exceeds the reliable range of AMS ^{14}C measurement. Stable oxygen and carbon isotopic ratios of planktonic foraminifera (*N. pachyderma*) were measured for a total of 54 samples at 15 cm intervals. Approximately 20 specimens of foraminifera were picked to analyze the isotopes using a mass spectrometer (MAT253) with the Kiel IV carbonate preparation system at Hokkaido University (Japan). The results were calibrated to the V-PDB standard using the standard NBS-19. The analytical precision, determined from the repeated measurements of standard was $\pm 0.05\text{ } \text{\textperthousand}$ for $\delta^{18}\text{O}$ and $\pm 0.03\text{ } \text{\textperthousand}$ for $\delta^{13}\text{C}$.

For the construction of the age model by comparison between the $\delta^{18}\text{O}$ record and LR04 stack (Lisiecki and Lisiecki, 2002), we utilized the Match program, which divides each normalized data series into hundreds of equal segments and uses the dynamic programming to decide the optimal alignment of the series. This approach allows a finer resolution in understanding the temporal dynamics of climate change.

3.2. Geochemical and isotopic analyses

For the geochemical properties (total carbon (TC), total nitrogen (TN), CaCO_3 , and biogenic opal) and $\delta^{13}\text{C}$ values of carbonate-free sediment organic matter (SOM) ($\delta^{13}\text{C}_{\text{SOM}}$), 54 sediment samples were collected at 15 cm intervals. TC and TN contents were determined using a Thermo Flash 2000 CHNS Elemental Analyzer at Pusan National University (Korea). The analytical precision of TC and TN content is $\pm 0.1\text{ } \text{\textperthousand}$. The total inorganic carbon (TIC) content was measured using a UIC CO₂ coulometer at Korea Institute of Ocean and Science Technology (Korea). The analytical precision of TIC content is $\pm 0.1\text{ } \text{\textperthousand}$. CaCO_3 content was calculated by multiplying TIC content by 8.333 (the mass ratio

of C to CaCO_3). Total organic carbon (TOC) content was calculated by the difference between TC and TIC contents. For the biogenic opal content, biogenic silica (Si_{Bio}) concentration was measured using a wet-alkaline sequential extraction method modified from DeMaster (1981) at Pusan National University (Korea). The analytical precision of the biogenic silica content is $\pm 1.0\text{ } \text{\textperthousand}$. The biogenic opal content was calculated by multiplying Si_{Bio} concentration by 2.4 (the mass ratio of Si_{Bio} to biogenic opal; Mortlock and Froelich, 1989). The $\delta^{13}\text{C}_{\text{SOM}}$ was measured using an elemental analysis-isotope ratio mass spectrometry (EA-IRMS: Europa Scientific 20–20 isotope ratio mass spectrometer) at Iso-Analytical Limited (UK). The results were calibrated to the V-PDB standard with an analytical precision of approximately $\pm 0.1\text{ } \text{\textperthousand}$.

3.3. Spectral and wavelet analyses

Spectral analysis on geochemical data was conducted using the REDFIT tool of the PAST statistics package (v. 4.03; Hammer, 2010). REDFIT is specifically designed to handle the noised data with irregular intervals (Schulz and Mudelsee, 2002). Linear interpolation was used to generate a set of 235 evenly spaced data points at 1 kyr interval, to preserve the original shape of the geochemical data curve for REDFIT analysis for significant periodicities. Blackman-Harris window function, an oversampling factor of 3, 1 segment, and without conducting Monte Carlo simulations were applied to calculate the REDFIT periodograms. These configurations were chosen to enhance the clarity of periodic signals within each geochemical parameter. In addition, wavelet analysis was applied to track variations in the frequency and amplitude of detected periodicities throughout the time series (Hammer, 2010).

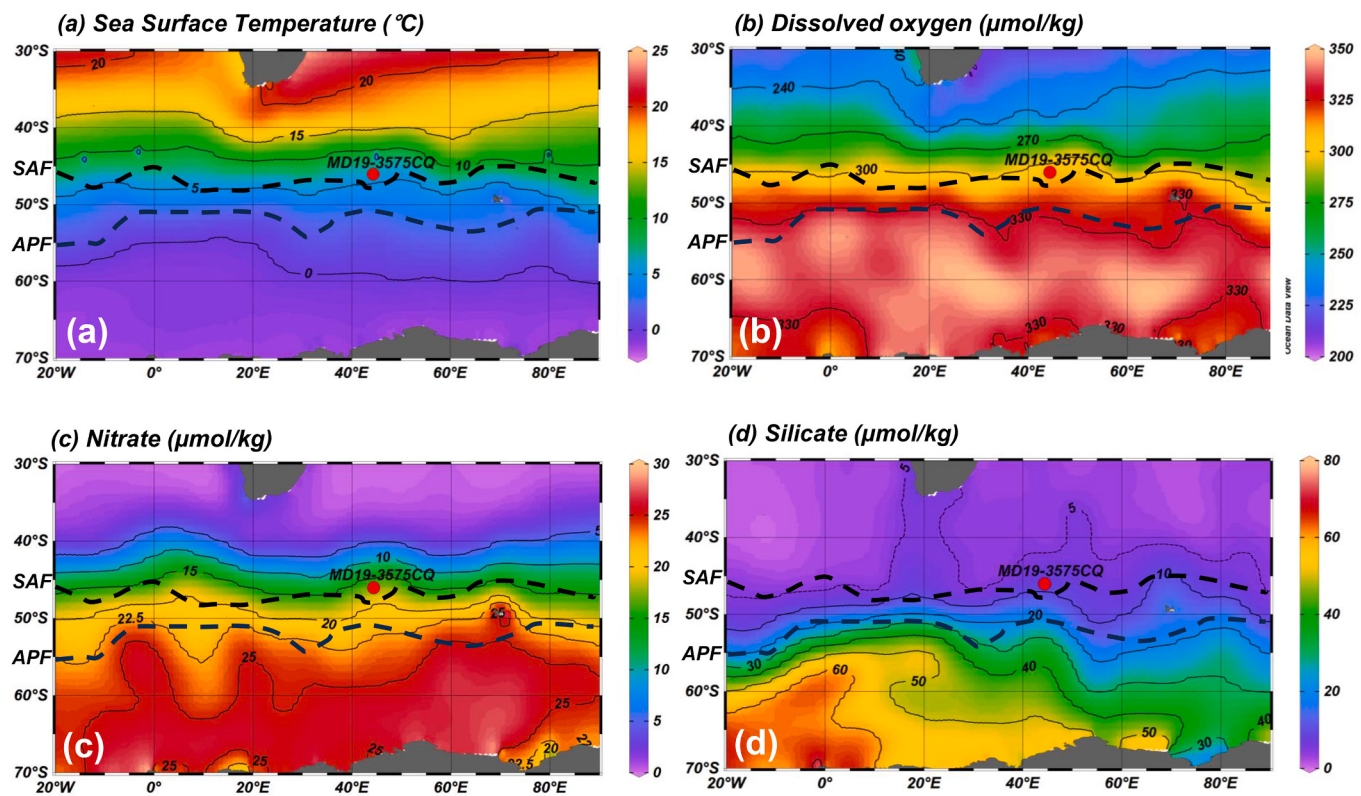


Fig. 2. Map showing (a) sea surface temperatures, (b) dissolved oxygen concentrations, (c) nitrate concentrations, and (d) silicate concentrations at the surface water (0 m) derived from World Ocean Atlas 2023 (Locarnini et al., 2024; Garcia et al., 2024a; Garcia et al., 2024b) with the location of core MG19-3575CQ.

4. Results

4.1. Age model and sedimentation rate

Table 1 summarizes the AMS ^{14}C ages obtained on core MD19-3575CQ. The AMS ^{14}C ages do not show any reversal, but the age at 155 cm older than 43,500 yr BP was discarded due to dating limitation. Older sediment ages were determined by the correlation of the $\delta^{18}\text{O}$ record of planktonic foraminifera to the LR04 stack (Lisiecki and Raymo, 2005). This resulted in thirteen tie points that date the bottom of core at ~ 235 kyr, thus reaching Marine Isotope Stage (MIS) 7 (Fig. 3). Our age model agrees with a previous chronology based on the tuning of the radiolarian inferred seawater temperature to EDC 8D record (Civelli-Mazens et al., 2024). Based on the chronological framework, the average sedimentation rate was about 3.2 cm/kyr. The sedimentation rate is slightly higher during the glacial periods (3.6 cm/kyr) than during the interglacial periods (2.9 cm/kyr) (Fig. 4).

4.2. Physical parameters

The core sediments consist of massive and foraminifera-bearing calcareous bioturbated silt alternating with diatomaceous silt to very

fine sand (Fig. 5; Crosta et al., 2019). Sediment colour and MS vary in agreement with the sediment composition (Fig. 5). Sediment colour L* (dark to light) and b* (blue to yellow) values generally show opposite trends that broadly correspond to the glacial-interglacial cycles: darker and bluer sediments (lower L* and higher b*) typically occur during the glacial periods whereas lighter and more yellowish sediments (higher L* and lower b*) occur during the interglacial periods. In contrast, a* (green to red) values follow a different downcore pattern that appears unrelated to the orbital-scale climate changes. Instead, the variability of a* values may reflect other factors such as organic matter content, iron oxide concentration, diagenetic alteration, and redox conditions (Nagao and Nakashima, 1992). MS fluctuations also follow the sediment colour change (Fig. 5). Low MS periods correspond to lighter and more yellowish sediments deposited during interglacial periods, whereas high MS layers coincide with the darker and less yellowish sediments deposited during glacial periods.

4.3. Geochemical proxies

All the analytical proxies of core MD19-3575CQ show distinct orbital-scale variations during the last 235 kyr (Fig. 6). The interglacial sediment layers, marked by high L* and low MS values, are

Table 1
AMS ^{14}C ages of core MD19-3575CQ.

Depth (cm)	Conventional ^{14}C age (yr BP)	Calibrated age (cal yr BP)	Calibrated age (cal yr BP)		Lab code
			1 sigma	2 sigma	
5	3620 ± 30	2766	2760–2832	2627–2917	Beta-638,366
20	6980 ± 30	6760	6672–6839	6600–6933	Beta-638,367
80	$26,570 \pm 120$	29,460	29,255–29,637	29,135–29,812	Beta-661,758
155	> 43500*	–	–	–	Beta-661,759

* Age older than 43,500 yr BP was not used to construct the age model due to the dating limitation.

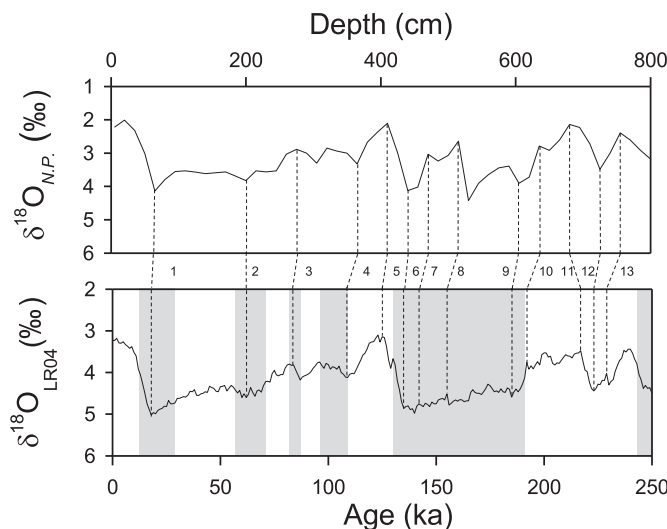


Fig. 3. Determination of chronological framework of core MD19-3575CQ by correlating its $\delta^{18}\text{O}$ record (*Neogloboquadrina pachyderma*) to the LR04 stack (Lisiecki and Raymo, 2005). Thirteen tie points (dashed lines) were decided by the correlation. The core bottom was estimated to date about 235 kyr. The shaded interval represents the glacial period based on the marine isotope stage (MIS).

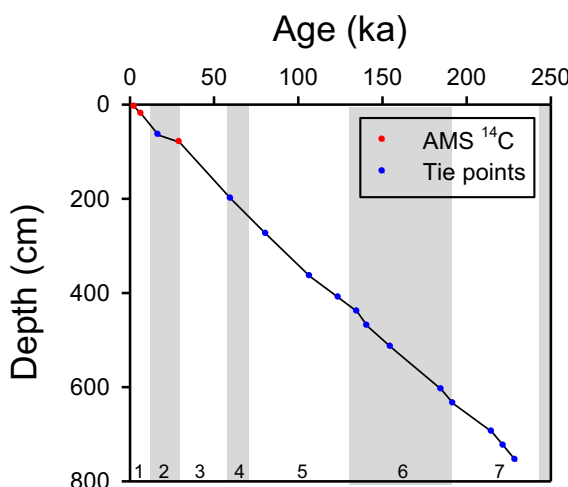


Fig. 4. Age-depth plot of core MD19-3575CQ based on Accelerator Mass Spectrometry (AMS) ^{14}C dates (red dots) and 13 tie points (black dots) that were decided in Fig. 3. The numbers below the segment line are the sedimentation rate (cm/ka) for each interval between the tie points. The horizontal small numbers indicated the marine isotope stage (MIS) and the shaded interval represents the glacial period. (For interpretation of the references to colour in this figure legend, the reader is referred to the web version of this article.)

characterized by low $\delta^{18}\text{O}$ values (ca. 2.7 ‰), high CaCO_3 (ca. 61.8 %), low biogenic opal (ca. 8.5 %), and low TOC (ca. 0.2 %) contents. The glacial sediment layers, corresponding to low L^* and high MS, are characterized by high $\delta^{18}\text{O}$ (ca. 3.5 ‰) values, low CaCO_3 (ca. 35.2 %), high biogenic opal (ca. 12.4 %), and high TOC (ca. 0.4 %) contents with small orbital-scale difference in the planktonic $\delta^{13}\text{C}$ and $\delta^{13}\text{Csom}$ (0.2 to 0.3 ‰) values. The CaCO_3 and biogenic opal records present an opposite relationship throughout the last 235 kyr, with a stronger negative relationship during the interglacial periods ($r^2 = 0.70$) compared to the glacial periods ($r^2 = 0.35$) (Fig. 7a). The relationship between biogenic opal and TOC contents is positive, with a stronger correlation during the glacial periods ($r^2 = 0.51$) than the interglacial periods ($r^2 = 0.07$) (Fig. 7b). More positive relationship reflects higher TOC burial in the

biogenic opal-dominated sediments. In contrast, the relationship between CaCO_3 and TOC contents is negative throughout the records (Fig. 7c), with a stronger negative correlation during the glacial periods ($r^2 = 0.69$) compared to the interglacial periods ($r^2 = 0.13$). It shows less TOC burial in biogenic carbonate-rich sediments different from the biogenic opal-dominated sediments. An abnormally high TOC value (0.90 %) at 590 cm depth (Fig. 6) seems outlier from the rest of results. This value was excluded in the correlation analysis to avoid distortion (Fig. 7a-c). As CaCO_3 content dominates biogenic opal content, the TOC content is also negatively related with the summation of biogenic opal and CaCO_3 contents (Fig. 7d).

4.4. Spectral and wavelet analyses

The stationary spectral analysis of the geochemical data exhibits distinct periodic peaks for CaCO_3 , biogenic opal, and TOC contents exceeding the 95 % confidence level (Fig. 8). These periodic peaks correspond to the eccentricity, obliquity, and precession cycles for CaCO_3 (107, 45, and 25 kyr), biogenic opal (149, 42, and 29 kyr), and TOC (125, 42, and 23 kyr). The wavelet analysis not only corroborates the REDFIT results but also illustrates the variations in the strength of these periodic signals during the last 235 kyr (Fig. 8). The wavelet analysis shows that the periodic signal of eccentricity near 100 kyr remained strong throughout the entire interval. In contrast, signals of obliquity and precession near 40 and 25 kyr, respectively, were more pronounced since ~150 kyr. Notably, the obliquity signal in the TOC record appears much stronger since ~50 kyr (Fig. 8f).

5. Discussion

5.1. Orbital-scale changes in biogenic carbonate and opal production at the Del Caño rise during the last 235 kyr

Currently, the phytoplankton productivity in the SAZ is dominated by coccolithophores because of high sea surface temperatures (SSTs) and low DSi availability preventing high diatom productivity (Bowie et al., 2011; Rigual-Hernández et al., 2015). Additionally, the carbonate preservation is facilitated at bathymetric highs, such as the Del Caño Rise, as the calcite saturation horizon lies at approximately 3400 m (Howard and Prell, 1994). Our results show high CaCO_3 and low biogenic opal contents in core MD19-3575CQ during the Holocene, MIS 5, and the early MIS 7 (Fig. 6), indicating that modern-like conditions prevailed during these warm periods (Civel-Mazens et al., 2024). CaCO_3 and biogenic opal records from the Atlantic and Pacific sectors of the SAZ show a similar pattern, confirming enhanced carbonate productivity during the interglacial periods (Fig. 9; Charles et al., 1991; Chase et al., 2003). These trends, however, should not be generalized to the entire Southern Ocean, as the dominant water mass structures across oceanic sectors and frontal zones can lead to contrasting productivity between glacial–interglacial periods (e.g., Charles et al., 1991; Manoj and Thamban, 2015; Tangunian et al., 2021). The pattern of these changes suggests high coccolithophore/foraminifera productivity and low diatom productivity during the interglacial periods. Although CaCO_3 content accounts for both coccoliths and foraminifera present in the sample, variations in CaCO_3 content within the SAZ in the Indian sector of the Southern Ocean are primarily influenced by coccolithophores (Flores et al., 2003; Brandon et al., 2022; Choudhari et al., 2023). This suggests that the DSi, supplied to Antarctic surface waters by the Southern Ocean upwelling in the ADZ, was rapidly depleted in the surface waters of the AZ by the diatoms as observed today (Tréguer, 2014). Consequently, little DSi could diffuse across the APF to the SAZ, leading to the low diatom productivity in the SAZ and little competition with coccolithophores for other nutrients (Fig. 10a).

Conversely, low CaCO_3 and high biogenic opal contents were recorded in core MD19-3575CQ during the glacial periods when SSTs were 4–5 °C lower than today (Fig. 6; Civel-Mazens et al., 2024) and the

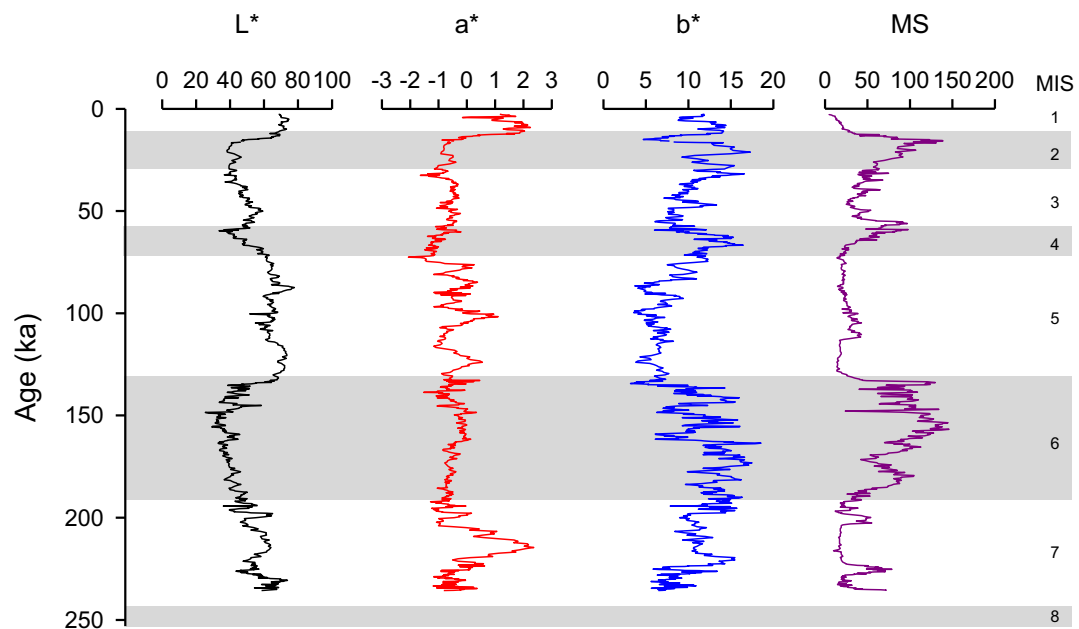


Fig. 5. Downcore variation of sediment colour (L^* : dark to light, a^* : blue to yellow, b^* : green to red) and magnetic susceptibility (MS) of core MD19-3575CQ. MIS was marked and the shaded interval represents the glacial period. (For interpretation of the references to colour in this figure legend, the reader is referred to the web version of this article.)

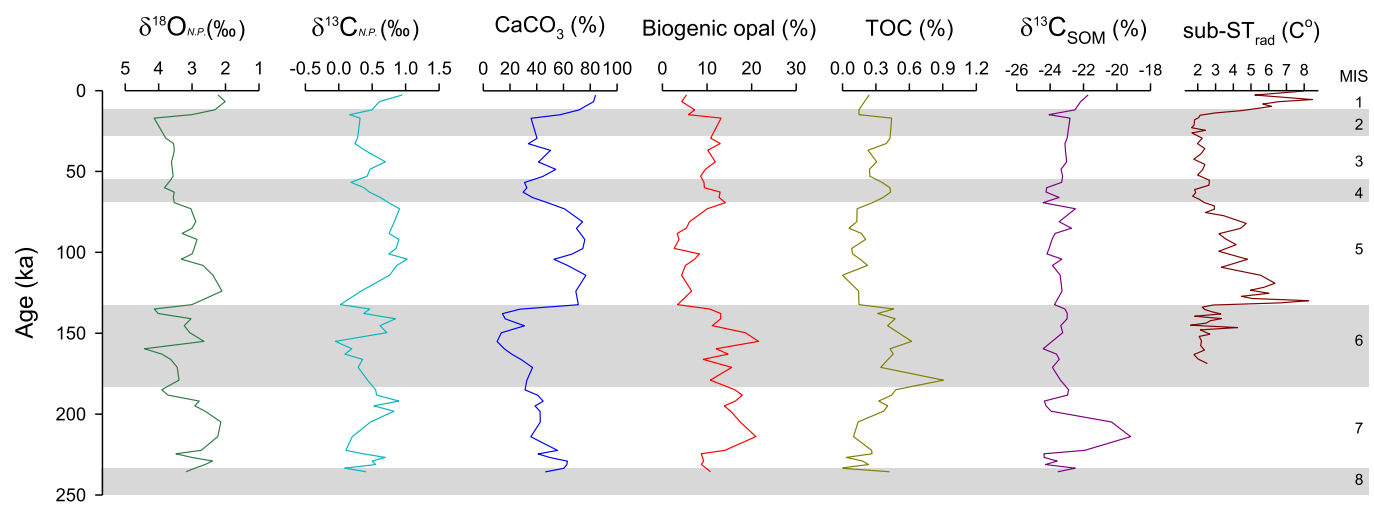


Fig. 6. Downcore profiles of $\delta^{18}\text{O}_{NP}$ and $\delta^{13}\text{C}_{NP}$ values of planktonic foraminifera (*Neogloboquadrina pachyderma*), CaCO_3 content, biogenic opal content, TOC content, $\delta^{13}\text{C}_{\text{SOM}}$ values, and sub-ST_{rad} ($^{\circ}\text{C}$) (Civel-Mazens et al., 2024) of core MD19-3575CQ, during the last 235 kyr. MIS was marked and the shaded interval represents the glacial period.

APF shifted northward from its modern position around the Conrad Rise to a position around the Del Caño Rise. Other regions in the SAZ of the Indian sector also exhibited a similar drop in CaCO_3 and increase in biogenic opal burial during the glacial periods (Fig. 9; Manoj and Thamban, 2015), suggesting a consistent glacial-interglacial productivity pattern within this sector. This suggests that a northward movement of the Southern Ocean upwelling accompanied the northward shift of APF, thus enabling higher DSi supply to surface waters over most regions in the SAZ (Fig. 10b). Due to the unavailability of DSi flux data in this region, a quantitative interpretation of DSi dynamics remains limited in this study. In addition, the Antarctic sea-ice cover was expanded during the glacial periods due to the combined effects of reduced insolation, lowered atmospheric temperature and SSTs, and decreased influx of CDW (Ferrari et al., 2014). In the Atlantic and

western Indian sectors of the Southern Ocean, winter sea-ice extent reached the present-day position of the APF during the Last Glacial Maximum (Gersonde et al., 2005). This northward expansion of sea-ice coverage during the glacial periods likely reduced diatom productivity in the region south of the study area, where the upwelled DSi was not consumed as much as during the interglacial periods, allowing more remained DSi to be transported northward toward the SAZ (Charles et al., 1991; Dezileau et al., 2003). The diatom productivity in the SAZ during the glacial periods likely intensified competition for light and nutrients with coccolithophores, thereby increasing their productivity (Fig. 10b), as also observed in previous studies reporting that diatom dominance under high nutrient conditions can suppress coccolithophore growth in the Southern Ocean (Quere et al., 2005; Sinha et al., 2010). Additionally, low SSTs during the glacial periods may have more

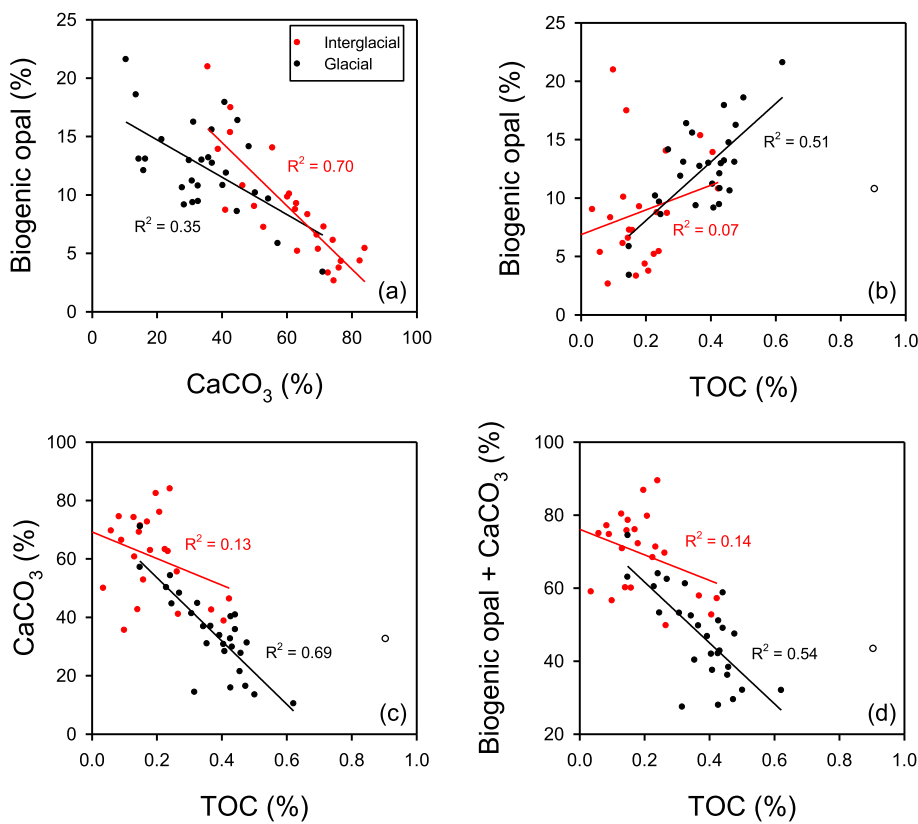


Fig. 7. Biplots of geochemical properties (CaCO_3 , biogenic opal, and TOC) with correlation coefficients of core MD19-3575CQ. The black and red circles represent the interglacial (MIS 1, 5, and 7) and glacial periods (MIS 2, 3, 4, and 6), respectively. Extraordinary high TOC sample (hollow circle) in (b), (c), and (d) was excluded in the calculation of correlation coefficient as an outlier. (For interpretation of the references to colour in this figure legend, the reader is referred to the web version of this article.)

suppressed the growth of the coccolithophorids and foraminifera, contributing to a decrease in CaCO_3 content in the sediments.

The transition from coccolithophore- to diatom-dominated communities, along with changes in carbonate and biogenic opal burial, indicates that surface water productivity was closely linked to the glacial-interglacial cycles. Spectral and wavelet analyses of CaCO_3 , biogenic opal, and TOC records support this linkage, showing the periodicities that align with eccentricity (100–125 kyr), obliquity (42–45 kyr), and precession (23–29 kyr) cycles (Fig. 8). These results suggest that variations in insolation, driven by orbital forcing, and the associated changes in oceanic front position, upwelling intensity, and sea-ice extent, were the key regulators of surface productivity and organic carbon burial in the SAZ over the past 235 kyr.

Lithogenic particles are transported to the Southern Ocean by diverse pathways including aeolian dust, ice-raftered debris, and sediment remobilization (Diekmann et al., 2000; Gaiero et al., 2004). The supply of Fe-bearing dust increased during the glacial periods, which has been considered a key factor in enhancing biological productivity in the Southern Ocean (Kumar et al., 1995; Lamy et al., 2014). However, the northward migration of the ACC and associated oceanic fronts during the glacial periods may have increased interactions with bathymetric highs. This may have enhanced Fe supply via a greater resuspension of the sediments deposited on Del Caño Rise and Crozet Plateau as well as a strengthening of the eddy field and regional upwelling (Tamsitt et al., 2017). Despite no characterization and quantification of lithogenic particles in core MD19-3575CQ, higher MS and increased sedimentation rate during the glacial periods suggest enhanced terrigenous supply to the core site, which may have contributed to the overall higher productivity as also evidenced by the TOC record. In this study, because Fe concentrations were not measured, all interpretations regarding Fe dynamics rely solely on the previously published data (Pollard et al.,

2009). Such limitations should be acknowledged as a constraint in the current analysis.

5.2. Orbital-scale changes in organic matter burial at the Del Caño rise during the last 235 kyr

TOC content of MD19-3575CQ was low during the interglacial periods and high during the glacial periods of the last 235 kyr (Fig. 6). Based on the $\delta^{13}\text{C}_{\text{OM}}$ values, the buried organic matter is mostly of marine origin, with minimal contribution from terrestrial organic matter or diagenetic alteration. Despite an unusual peak of high $\delta^{13}\text{C}_{\text{OM}}$ values during MIS 7 (Fig. 6). However, due to a lack of supporting data, its cause remains unclear and is not interpreted farther. Variations in TOC content in core MD19-3575CQ, with a mean value of 0.5 % and 0.3 %, respectively, during the glacial and interglacial periods, are broadly consistent with the records from other parts in the SAZ of the Indian sector such as the Agulhas Plateau, north of the Crozet Archipelago, and north of the Kerguelen Plateau (Fig. 11). Notably, during MIS 7, CaCO_3 and biogenic opal contents varied independently of the glacial-interglacial cycles. In contrast, TOC follows the glacial-interglacial cycle, with higher during the glacial periods and lower during the interglacial periods. This discrepancy may reflect localized productivity changes driven by oceanic front migrations interacting with bathymetric highs. In fact, Shukla et al. (2023), based on core MD11-3357 recovered from the same area, suggested that enhanced diatom productivity during MIS 5 and 7 was associated with the frontal movement and topographically-induced upwelling. A similar mechanism might have also contributed to the anomalous CaCO_3 and biogenic opal signals at our study site. Hence, TOC variations are more plausibly linked to the glacial-interglacial differences in organic matter preservation. This interpretation is addressed in more detail later.

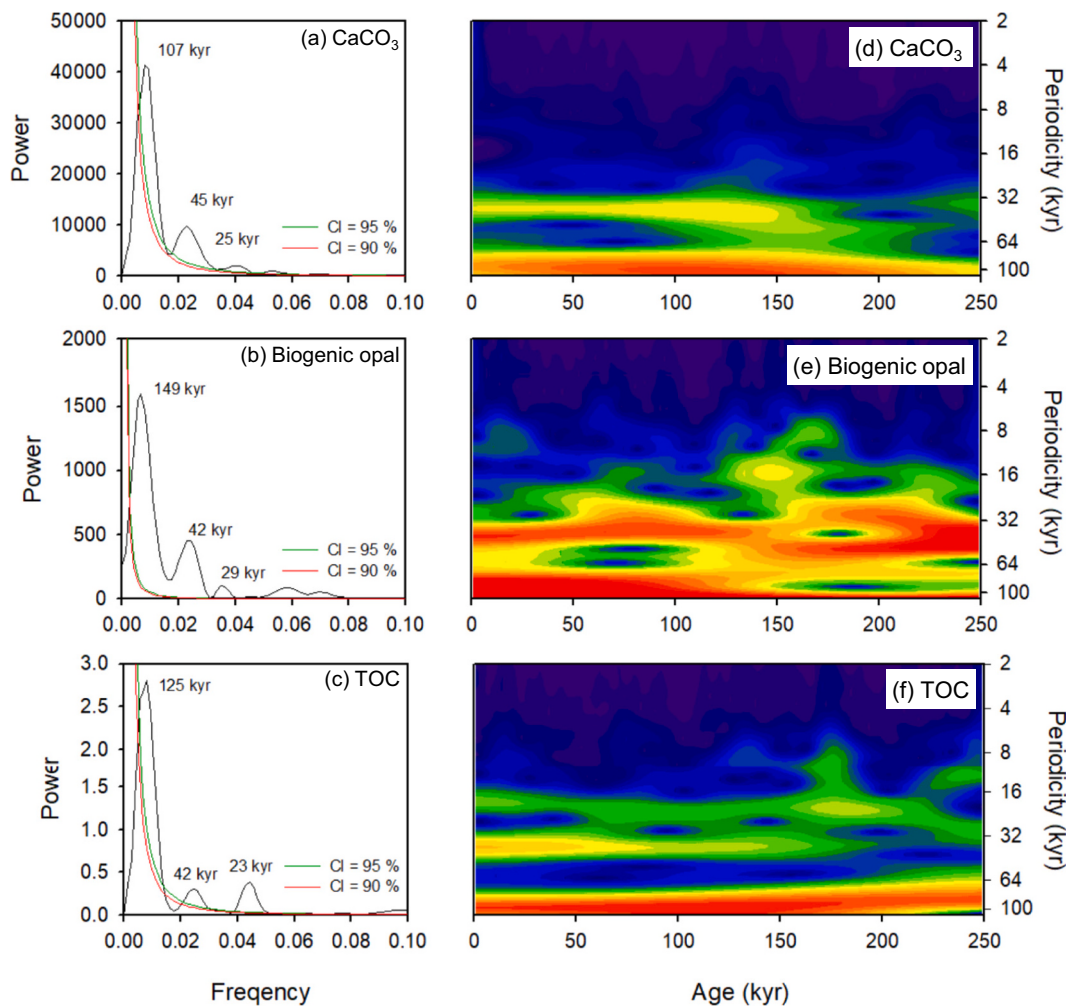


Fig. 8. Results of the REDFIT spectral analysis (a: CaCO_3 content, b: biogenic opal content, and c: TOC content) and wavelet analysis (d: CaCO_3 content, e: biogenic opal content, and f: TOC content) of MD19-3575CQ during the last 235 kyr. The 90 % and 95 % confidence levels are indicated by the green and red lines, respectively. (For interpretation of the references to colour in this figure legend, the reader is referred to the web version of this article.)

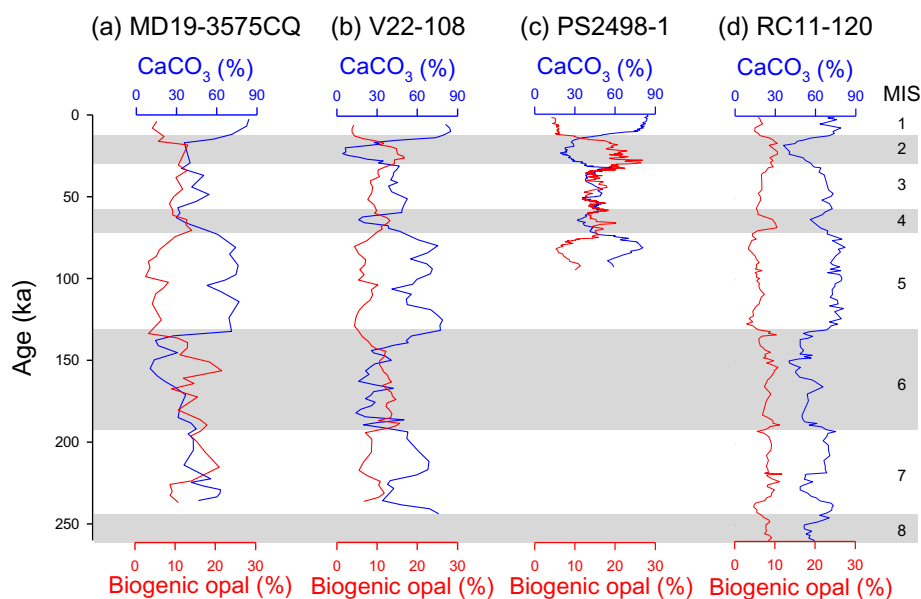


Fig. 9. Comparison of downcore profiles of CaCO_3 and biogenic opal contents of the Subantarctic Zone during the last 235 kyr: (a) MD19-3575CQ (this study), (b) V22-108 (Charles et al., 1991), (c) PS2498-1 (Anderson et al., 2014), and (d) RC11-120 (Charles et al., 1991). Core locations refer to Fig. 1. MIS was marked and the shading represents the glacial periods.

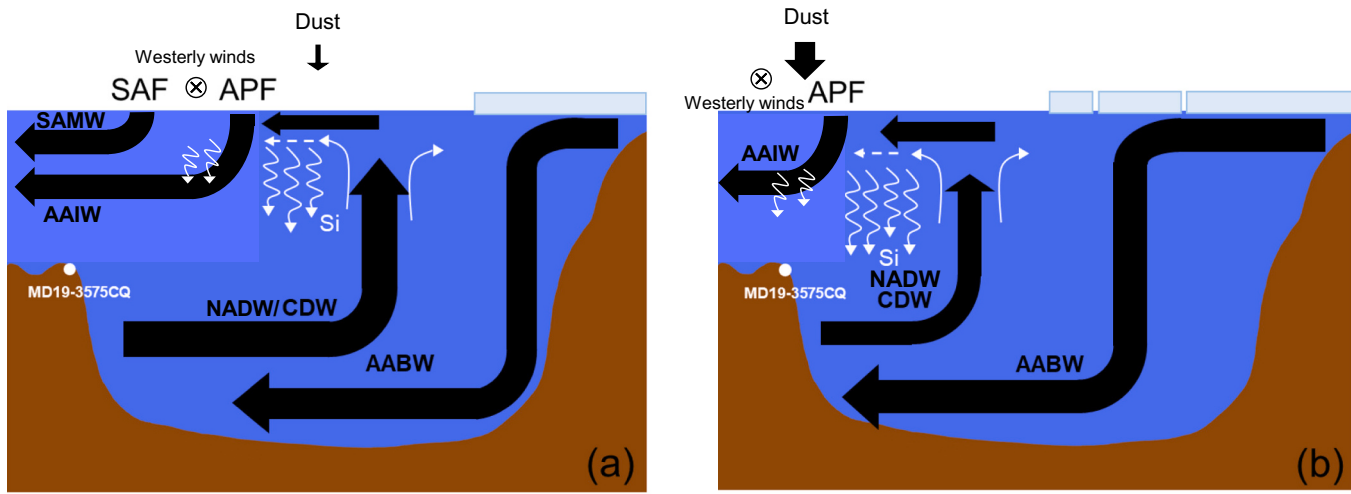


Fig. 10. Schematic conceptual model showing the paleoceanographic environmental change between (a) interglacial and (b) glacial periods in the southwestern Indian sector of the Southern Ocean. Black arrows represent the ocean circulation and dust input. White arrows indicate the supply and transport of silica (Si). Sky-blue boxes represent the sea ice cover. AABW: Antarctic Bottom Water, CDW: Circumpolar Deep Water, AAIW: Antarctic Intermediate Water, SAMW: Subantarctic Mode Water, SAF: Subantarctic Polar Front, APF: Antarctic Polar Front. (For interpretation of the references to colour in this figure legend, the reader is referred to the web version of this article.)

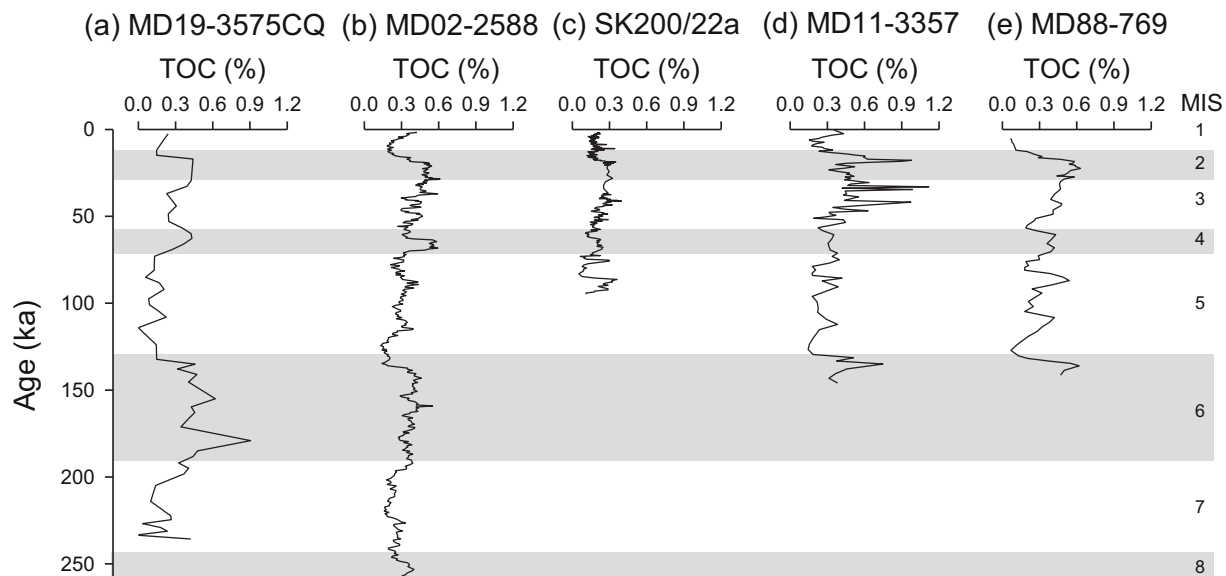


Fig. 11. Comparison of downcore profiles of TOC in the Subantarctic Zone during the last 235 kyr: (a) MD19-3575CQ (this study), (b) MD02-2588 (Romero et al., 2015), (c) SK200/22a (Manoj and Thamban, 2015), (d) MD11-3357 (Thöle et al., 2019) and (e) MD88-769 (Rosenthal et al., 1995). Core locations refer to Fig. 1. MIS was marked and shading represents the glacial periods.

In core MD19-3575CQ, the relationship between the biogenic opal and TOC contents is positively linear, with higher correlation coefficient during the glacial periods (Fig. 7b). It indicates that the export organic matter and burial are closely related to diatom productivity, although biogenic opal content is not the main productivity component. It also reflects that, during the glacial periods, increased diatom productivity led to greater export production and enhanced TOC preservation (e.g. Manoj and Thamban, 2015; Shukla et al., 2023). Furthermore, the increased influx of lithogenic particles during the glacial periods may have amplified the ballast effect, thereby accelerating sinking speed and protecting organic matter from degradation (Armstrong et al., 2001). In contrast, the relationship between CaCO_3 and TOC contents is negative across all periods (Fig. 7c), indicating that coccoliths and foraminifera had little impact on organic matter export and burial at the core site. During the glacial periods, this negative correlation is stronger, likely

due to increased diatom productivity outcompeting coccolithophores for nutrients, thereby suppressing carbonate production. In contrast, during the interglacial periods, when coccolithophore productivity was higher (e.g., Choudhari et al., 2023), the weaker correlation between CaCO_3 and TOC suggests that TOC preservation was influenced by factors other than surface water productivity (Fig. 7c). This interpretation leads to the consideration that the reduced preservation of organic matter rather than decreased production may have limited TOC accumulation during the interglacial periods.

During glacial periods, the weakened Atlantic Meridional Overturning Circulation likely reduced deep water ventilation and created reducing conditions in the bottom waters overlying the seafloor (Gottschalk et al., 2020). On the other hand, during the interglacial periods, enhanced ocean circulation and upwelling could have led to the re-oxygenation of bottom waters in the Southern Ocean (Skinner et al.,

2010). We hypothesized that the low correlation between biogenic opal and TOC contents as well as the poor correlation between CaCO_3 and TOC contents during interglacial periods are linked to the significant degradation of organic matter under enhanced bottom water oxygenation. Amsler et al. (2022) reported the pronounced changes of glacial-interglacial bottom water oxygenation in the southwestern Indian Ocean, including the Del Caño Rise, inferred from redox-sensitive elemental records. Their findings support the hypothesis that reduced deep-water ventilation during the glacial periods intensified organic carbon preservation by limiting oxygen availability within the sediments. Thus, TOC burial in the study area is mainly dependent on surface water production and export during glacial periods and bottom water degradation during interglacial periods.

Our results suggest that the SAZ in the Indian sector of the Southern Ocean responds to glacial–interglacial climate cycles through the periodic environmental changes that drive consequential shift in biological productivity and organic carbon burial dynamics. During the glacial periods, surface water productivity in the SAZ was dominated by diatoms and organic matter was effectively transferred to the seafloor. This efficient export may have been supported by a ballast effect from higher terrigenous input. As a result, the BCP was likely enhanced during the glacial periods. In contrast, during the interglacial periods, calcifying organisms such as coccolithophores and foraminifera dominated. However, their impact on atmospheric CO_2 drawdown seems reduced due to the counteracting effect of the CCP, which offsets photosynthetic CO_2 uptake (Duchamp-Alphonse et al., 2018). Furthermore, the release of CO_2 from the ocean to the atmosphere may have been promoted during the interglacial periods by the enhanced oxygenation of bottom water, reduced gradient of vertical density, and stronger upwelling (Skinner et al., 2010). Studies on coccolithophore, foraminifera, and diatom physiology (calcification and silicification) and biometry (size and biovolume) would be necessary to refine the role of each group on TOC burial and CO_2 partitioning.

6. Conclusions

The Southern Ocean's distinct oceanic fronts have undergone significant glacial and interglacial shifts, profoundly influencing the global carbon cycle. The present study reconstructed phytoplankton productivity changes in the Subantarctic Zone (SAZ) of the southwestern Indian Ocean, using biogenic components (CaCO_3 , biogenic opal, and TOC), over the last 235 kyr. Our results reveal orbital-scale opposite cyclic changes in CaCO_3 and biogenic opal contents. Interglacial periods were characterized by high CaCO_3 content in response to coccolithophore and foraminifera productivity and low biogenic opal content by diatom productivity. In contrast, glacial periods featured increased biogenic opal content probably because of intensified diatom productivity, driven by increased Si and Fe supply. High diatom productivity led to higher TOC burial through enhanced export production and ballast effect. The weak biogenic opal-TOC and CaCO_3 -TOC correlations during interglacial periods suggest that organic carbon preservation was influenced by other factors beyond surface water productivity. More oxygenated bottom waters, related to the upwelling of Circumpolar Deep Water, probably increased TOC degradation. These findings highlight the crucial role of diatom-driven BCP during glacial periods in storing organic carbon and reducing atmospheric CO_2 , emphasizing the SAZ's dynamic impact on the carbon cycle. In the SAZ in the Indian sector of the Southern Ocean, the paleoenvironmental reconstruction based on combined CaCO_3 and biogenic opal records are extremely rare. Thus, our study provides valuable insights into the regional productivity changes and their implications for the past carbon cycle.

CRediT authorship contribution statement

Hyuk Choi: Writing – original draft, Visualization, Methodology, Formal analysis, Data curation. **Xavier Crosta:** Writing – review &

editing, Validation, Resources, Investigation. **Isabelle Billy:** Validation, Formal analysis, Data curation. **Tomohisa Irino:** Validation, Formal analysis, Data curation. **Sangbeom Ha:** Validation, Investigation. **Hiro-yuki Takata:** Validation, Formal analysis, Data curation. **Boo-Keun Khim:** Writing – review & editing, Validation, Funding acquisition, Conceptualization.

Declaration of competing interest

The authors declare that they have no known competing financial interests or personal relationships that could have appeared to influence the work reported in this paper.

Acknowledgments

We thank the captain, crew, and all onboard technicians and researchers of MD218 CROTALE cruise for collecting the cores using R/V *Marion Dufresne*, which was funded by the Flotte Océanographique Française and supported by the EquipEx CLIMCOR (ANR-11-EQPX-0009- CLIMCOR). Graduate student (Ms. J.Y. Yang) of Pusan National University was appreciated for the laboratory works. Two anonymous reviewers were greatly appreciated on their constructive and valuable comments to improve the manuscript. This work was supported by National Research Foundation of Korea (2022R1A2B5B01001811, RS-2024-00436001) and Korea Institute of Marine Science & Technology funded by the Ministry of Oceans and Fisheries (RS-2023-00256330).

Appendix A. Supplementary data

Supplementary data to this article can be found online at <https://doi.org/10.1016/j.palaeo.2025.113290>.

Data availability

Datasets are available in the Supplementary Material.

References

- Amsler, H.E., Thöle, L.M., Stimac, I., Geibert, W., Ikebara, M., Kuhn, G., Esper, O., Jaccard, S.L., 2022. Bottom water oxygenation changes in the southwestern Indian Ocean as an indicator for enhanced respired carbon storage since the last glacial inception. *Clim. Past* 18, 1797–1813. <https://doi.org/10.5194/cp-18-1797-2022>.
- Anderson, R.F., Barker, S., Fleisher, M., Gersonde, R., Goldstein, S.L., Kuhn, G., Mortyn, P.G., Pahnke, K., Sachs, J.P., 2014. Biological response to millennial variability of dust and nutrient supply in the Subantarctic South Atlantic Ocean. *Philos. Trans. R. Soc. A* 372, 20130054. <https://doi.org/10.1098/rsta.2013.0054>.
- Armstrong, R.A., Lee, C., Hedges, J.I., Honjo, S., Wakeham, S.G., 2001. A new, mechanistic model for organic carbon fluxes in the ocean based on the quantitative association of POC with ballast minerals. *Deep-Sea Res. II* 49, 219–236. [https://doi.org/10.1016/S0967-0645\(01\)00101-1](https://doi.org/10.1016/S0967-0645(01)00101-1).
- Balch, W.M., Drapeau, D.T., Bowler, B.C., Lyczkowski, E., Booth, E.S., Alley, D., 2011. The contribution of coccolithophores to the optical and inorganic carbon budgets during the Southern Ocean Gas exchange experiment: new evidence in support of the “Great Calcite Belt” hypothesis. *J. Geophys. Res. (Oceans)* 116, C00F06. <https://doi.org/10.1029/2011JC006941>.
- Bowie, A.R., Griffiths, F.B., Dehairs, F., Trull, T.W., 2011. Oceanography of the subantarctic and Polar Frontal zones south of Australia during summer: setting for the SAZ-Sense study. *Deep-Sea Res. II* 58, 2059–2070. <https://doi.org/10.1016/j.dsr2.2011.05.033>.
- Boyd, P.W., Newton, P.P., 1999. Does planktonic community structure determine downward particulate organic carbon flux in different oceanic provinces? *Deep-Sea Res. I* 46, 63–91. [https://doi.org/10.1016/S0967-0637\(98\)00066-1](https://doi.org/10.1016/S0967-0637(98)00066-1).
- Brandon, M., Duchamp-Alphonse, S., Michel, E., Landais, A., Isguder, G., Richard, P., Pige, N., Bassinot, F., Jaccard, S., Bartolini, A., 2022. Enhanced carbonate counter pump and upwelling strengths in the Indian sector of the Southern Ocean during MIS 11. *Quat. Sci. Rev.* 287. <https://doi.org/10.1016/j.quascirev.2022.107556>.
- Charles, C.D., Froelich, P.N., Zibello, M.A., Mortlock, R.A., Morley, J.J., 1991. Biogenic opal in Southern Ocean sediments over the last 450,000 years: Implications for surface water chemistry and circulation. *Paleoceanography* 6, 697–728. <https://doi.org/10.1029/91PA02477>.
- Chase, Z., Anderson, R.F., Fleisher, M.Q., Kubik, P.W., 2003. Accumulation of biogenic and lithogenic material in the Pacific sector of the Southern Ocean during the past 40,000 years. *Deep-Sea Res. II* 50, 799–832. [https://doi.org/10.1016/S0967-0645\(02\)00595-7](https://doi.org/10.1016/S0967-0645(02)00595-7).

- Choudhari, P., Nair, A., Mohan, R., Patil, S., 2023. Variations in the Southern Ocean carbonate production, preservation, and hydrography for the past 41,500 years: evidence from coccolith and CaCO₃ records. *Palaeogeogr. Palaeoclimatol. Palaeoecol.* 614, 111425. <https://doi.org/10.1016/j.palaeo.2023.111425>.
- Civell-Mazens, M., Crosta, X., Cortese, G., Lowe, V., Itaki, T., Ikebara, M., Kohfeld, K., 2024. Subantarctic jet migrations regulate vertical mixing in the Southern Indian. *Earth Planet. Sci. Lett.* 642, 118877. <https://doi.org/10.1016/j.epsl.2024.118877>.
- Crosta, X., Debret, M., Denis, D., Courte, M.A., Ther, O., 2007. Holocene long- and short-term climate changes off Adélie Land, East Antarctica. *Geochem. Geophys. Geosyst.* 8, Q11009. <https://doi.org/10.1029/2007GC001718>.
- Crosta, X., Read, Y., Landreau, F., 2019. MD218 CROTALE Expedition cruise report. Doctoral dissertation, EPOC 5805 – Environnements et Paléoenvironnements Océaniques, Univ. Bordeaux.
- DeMaster, D.J., 1981. The supply and accumulation of silica in the marine environment. *Geochim. Cosmochim. Acta* 45, 1715–1732. [https://doi.org/10.1016/0016-7037\(81\)90006-5](https://doi.org/10.1016/0016-7037(81)90006-5).
- Desileau, L., Reys, J., Lemoine, F., 2003. Late Quaternary changes in biogenic opal fluxes in the Southern Indian Ocean. *Mar. Geol.* 202, 143–158. [https://doi.org/10.1016/S0025-3227\(03\)00283-4](https://doi.org/10.1016/S0025-3227(03)00283-4).
- Diekmann, B., Kuhn, G., Rachold, V., Abelmann, A., Brathauer, U., Fütterer, D.K., Gersonne, R., Grobe, H., 2000. Terrigenous sediment supply in the Scotia Sea (Southern Ocean): response to late Quaternary ice dynamics in Patagonia and on the Antarctic Peninsula. *Palaeogeogr. Palaeoclimatol. Palaeoecol.* 162, 357–387. [https://doi.org/10.1016/S0031-0182\(00\)00138-3](https://doi.org/10.1016/S0031-0182(00)00138-3).
- Duchamp-Alphonse, S., Siani, G., Michel, E., Beaufort, L., Gally, Y., Jaccard, S.L., 2018. Enhanced Ocean-atmosphere carbon partitioning via the carbonate counter pump during the last deglacial. *Nat. Commun.* 9, 2396. <https://doi.org/10.1038/s41467-018-04625-7>.
- Ferrari, R., Jansen, M.F., Adkins, J.F., Burke, A., Stewart, A.L., Thompson, A.F., 2014. Antarctic Sea ice control on ocean circulation in present and glacial climates. *Proc. Natl. Acad. Sci.* 111, 8753–8758. <https://doi.org/10.1073/pnas.1323922111>.
- Flores, J.A., Marino, M., Sierra, F.J., Hodell, D.A., Charles, C.D., 2003. Calcareous plankton distribution pattern and coccolithophore assemblages during the last 600 kyr at ODP Site 1089 (Cape Basin, South Atlantic): paleoceanographic implications. *Palaeogeogr. Palaeoclimatol. Palaeoecol.* 196, 409–426 doi: 10.1016/S0031-0182(03)00467-X.
- Gaiero, D.M., Depetris, P.J., Probst, J.L., Bidart, S.M., Leleyter, L., 2004. The signature of river-and-wind-borne materials exported from Patagonia to the southern latitudes: a view from REEs and implications for paleoclimatic interpretations. *Earth Planet. Sci. Lett.* 219, 357–376. [https://doi.org/10.1016/s0012-821x\(03\)00686-1](https://doi.org/10.1016/s0012-821x(03)00686-1).
- Garcia, H.E., Bouchard, C., Cross, S.L., Paver, C.R., Reagan, J.R., Boyer, T.P., Locarnini, R.A., Mishonov, A.V., Baranova, O.K., Seidov, D., Wang, Z., Dukhovskoy, D., 2024a. World Ocean Atlas 2023, volume 4: dissolved inorganic nutrients (Phosphate, Nitrate, and Silicate). NOAA Atlas NESDIS 92. <https://doi.org/10.25923/39qw-7j08>.
- Garcia, H.E., Wang, Z., Bouchard, C., Cross, S.L., Paver, C.R., Reagan, J.R., Dukhovskoy, D., 2024b. World Ocean Atlas 2023, volume 3: dissolved oxygen, apparent oxygen utilization, dissolved oxygen saturation and 30-year climate normal. NOAA Atlas NESDIS 91. <https://doi.org/10.25923/rb67-ns53>.
- Gersonne, R., Crosta, X., Abelmann, A., Armand, L., 2005. Sea-surface temperature and sea ice distribution of the Southern Ocean at the EPILOG last Glacial Maximum—a circum-Antarctic view based on siliceous microfossil records. *Quat. Sci. Rev.* 24, 869–896. <https://doi.org/10.1016/j.quascirev.2004.07.015>.
- González-Dávila, M., Santana-Casiano, J.M., Fine, R., Happell, J., Delille, B., Speich, S., 2011. Carbonate system in the water masses of the Southeast Atlantic sector of the Southern Ocean during February and March 2008. *Biogeosciences* 8, 1401–1413. <https://doi.org/10.5194/bg-8-1401-2011>.
- Gottschalk, J., Hodell, D.A., Skinner, L.C., Crowhurst, S.J., Jaccard, S.L., Charles, C., 2018. Past carbonate preservation events in the deep Southeast Atlantic Ocean (Cape Basin) and their implications for Atlantic overturning dynamics and marine carbon cycling. *Paleoceanogr. Paleoclimatol.* 33, 643–663. <https://doi.org/10.1029/2018PA003353>.
- Gottschalk, J., Skinner, L.C., Jaccard, S.L., Menvil, L., Nehrbass-Ahles, C., Waelbroeck, C., 2020. Southern Ocean link between changes in atmospheric CO₂ levels and northern-hemisphere climate anomalies during the last two glacial periods. *Quat. Sci. Rev.* 230, 106067. <https://doi.org/10.1016/j.quascirev.2019.106067>.
- Hammer, Ø., 2010. PAST 2.04-Paleontological Statistics. <http://www.toyen.uio.no/~ohammer/past>.
- Heaton, T.J., Köhler, P., Butzin, M., Bard, E., Reimer, R.W., Austin, W.E., Ramsey, C.B., Grootes, P.M., Hughen, K.A., Kromer, B., 2020. Marine20—the marine radiocarbon age calibration curve (0–55,000 cal BP). *Radiocarbon* 62, 779–820. <https://doi.org/10.1017/rdc.2020.68>.
- Holligan, P.M., Charalampopoulou, A., Hutson, R., 2010. Seasonal distribution of the coccolithophore *Emiliania huxleyi* and of particulate inorganic carbon in the surface waters of the Scotia Sea. *J. Mar. Syst.* 82, 195–205. <https://doi.org/10.1016/j.jmarsys.2010.05.007>.
- Howard, W.R., Prell, W.L., 1994. Late Quaternary CaCO₃ production and preservation in the Southern Ocean: Implications for oceanic and atmospheric carbon cycling. *Paleoceanography* 9, 453–482. <https://doi.org/10.1029/93pa03524>.
- Jaccard, S.L., Hayes, C.T., Martínez-García, A., Hodell, D.A., Anderson, R.F., Sigman, D. M., Haug, G.H., 2013. Two modes of change in Southern Ocean productivity over the past million years. *Science* 339, 1419–1423. <https://doi.org/10.1126/science.1227545>.
- Kumar, N., Anderson, R., Mortlock, R., Froelich, P., Kubik, P., Dittrich-Hannen, B., Suter, M., 1995. Increased biological productivity and export production in the glacial Southern Ocean. *Nature* 378, 675–680. <https://doi.org/10.1038/378675a0>.
- Lamy, F., Gersonne, R., Winckler, G., Esper, O., Jaeschke, A., Kuhn, G., Ullermann, J., Martínez-García, A., Lambert, F., Kilian, R., 2014. Increased dust deposition in the Pacific Southern Ocean during glacial periods. *Science* 343, 403–407. <https://doi.org/10.1126/science.1245424>.
- Lisiecki, L.E., Lisiecki, P.A., 2002. Application of dynamic programming to the correlation of paleoclimate records. *Paleoceanography* 17, 1–1–1–12. <https://doi.org/10.1029/2001pa000733>.
- Lisiecki, L.E., Raymo, M.E., 2005. A Pliocene-Pleistocene stack of 57 globally distributed benthic $\delta^{18}\text{O}$ records. *Paleoceanography* 20, PA1003. <https://doi.org/10.1029/2004pa001071>.
- Locarnini, R.A., Mishonov, A.V., Baranova, O.K., Reagan, J.R., Boyer, T.P., Seidov, D., Wang, Z., Garcia, H.E., Bouchard, C., Cross, S.L., Paver, C.R., Dukhovskoy, D., 2024. World Ocean Atlas 2023, volume 1: temperature. NOAA Atlas NESDIS 89, 52. <https://doi.org/10.25923/54bh-1613>.
- Manoj, M., Thamban, M., 2015. Shifting frontal regimes and its influence on bioproductivity variations during the late Quaternary in the Indian sector of Southern Ocean. *Deep-Sea Res. II* 118, 261–274. <https://doi.org/10.1016/j.dsr2.2015.03.011>.
- Martínez-García, A., Sigman, D.M., Ren, H., Anderson, R.F., Straub, M., Hodell, D.A., Jaccard, S.L., Eglinton, T.I., Haug, G.H., 2014. Iron fertilization of the Subantarctic Ocean during the last ice age. *Science* 343, 1347–1350. <https://doi.org/10.1126/science.124684>.
- Mortlock, R.A., Froelich, P.N., 1989. A simple method for the rapid determination of biogenic opal in pelagic marine sediments. *Deep-Sea Res. A* 36, 1415–1426. [https://doi.org/10.1016/0198-0149\(89\)90092-7](https://doi.org/10.1016/0198-0149(89)90092-7).
- Nagao, S., Nakashima, S., 1992. The factors controlling vertical color variations of North Atlantic Madeira Abyssal Plain sediments. *Mar. Geol.* 109, 83–94. [https://doi.org/10.1016/0025-3227\(92\)90222-4](https://doi.org/10.1016/0025-3227(92)90222-4).
- Nair, A., Ghadi, P., Mohan, R., Manoj, M.C., Crosta, X., Shukla, S.K., Thamban, M., 2020. Glacial-interglacial flux and size variability of *Fragilaropsis kerguelensis* and *Thalassiosira lentiginosa* from the Indian sector of the Southern Ocean. *Deep-Sea Res. II* 178, 104746. <https://doi.org/10.1016/j.dsr2.2020.104746>.
- Orsi, A.H., Whitworth III, T., Nowlin Jr., W.D., 1995. On the meridional extent and fronts of the Antarctic Circumpolar current. *Deep-Sea Res. I* 42, 641–673. [https://doi.org/10.1016/0967-0637\(95\)00021-w](https://doi.org/10.1016/0967-0637(95)00021-w).
- Pollard, R.T., Salter, I., Sanders, R.J., Lucas, M.I., Moore, C.M., Mills, R.A., Statham, P.J., Allen, J.T., Baker, A.R., Bakker, D.C.E., Charette, M.A., Fielding, S., Fones, G.R., French, M., Hickman, A.E., Holland, R.J., Hughes, J.A., Jickells, T.D., Lampitt, R.S., Morris, P.J., Nédélec, F.H., Nielsdóttir, M., Planquette, H., Popova, E.E., Poultney, A. J., Read, J.F., Seeyave, S., Smith, T., Stinchcombe, M., Taylor, S., Thomalla, S., Venables, H.J., Williamson, R., Zubkov, M.V., 2009. Southern Ocean deep-water carbon export enhanced by natural iron fertilization. *Nature* 457, 577–580. <https://doi.org/10.1038/nature07716>.
- Quere, C.L., Harrison, S.P., Colin Prentice, I., Buitenhuis, E.T., Aumont, O., Bopp, L., Hervé, C., Cotrim da Cunha, L., Geider, R., Giraud, X., Klaas, C., Kohfeld, K.E., Legendre, L., Manizza, M., Platt, T., Rivkin, R.B., Sathyendranath, S., Utz, J., Watson, A.J., Wolf-Gladrow, D., 2005. Ecosystem dynamics based on plankton functional types for global ocean biogeochemistry models. *Glob. Chang. Biol.* 11, 2016–2040. <https://doi.org/10.1111/j.1365-2486.2005.1004.x>.
- Rigual-Hernández, A., Trull, T.W., Bray, S., Cortina, A., Armand, L., 2015. Latitudinal and temporal distributions of diatom populations in the pelagic waters of the Subantarctic and Polar Frontal zones of the Southern Ocean and their role in the biological pump. *Biogeosciences* 12, 5309–5337. <https://doi.org/10.5194/bg-12-5309-2015>.
- Rigual-Hernández, A.S., Trull, T.W., Nodder, S.D., Flores, J.A., Bostock, H., Abrantes, F., Eriksen, R.S., Sierra, F.J., Davies, D.M., Ballegeer, A.M., Fuertes, M.A., Northcote, L. C., 2020. Coccolithophore biodiversity controls carbonate export in the Southern Ocean. *Biogeosciences* 17, 245–263. <https://doi.org/10.5194/bg-17-245-2020>.
- Rintoul, S.R., Garabato, A.C.N., 2013. Dynamics of the Southern Ocean circulation. In: Siedler, G., Griffies, S.M., Gould, J., Church, J.A. (Eds.), *Ocean Circulation and Climate: A 21st Century Perspective*. International Geophysics, vol. 103. Academic Press, pp. 471–492. <https://doi.org/10.1016/B978-0-12-391851-2.00018-0>.
- Rintoul, S.R., Hughes, C.W., Olbers, D., 2001. The Antarctic circumpolar current system. In: Siedler, G., Church, J., Gould, J. (Eds.), *Ocean Circulation and Climate: Observing and Modelling the Global Ocean*, International Geophysics Series, vol. 77, pp. 271–302. [https://doi.org/10.1016/S0074-6142\(01\)80124-8](https://doi.org/10.1016/S0074-6142(01)80124-8).
- Romero, O.E., Kim, J.H., Bárcena, M.A., Hall, I.R., Zahn, R., Schneider, R., 2015. High-latitude forcing of diatom productivity in the southern Agulhas Plateau during the past 350 kyr. *Paleoceanography* 30, 118–132. <https://doi.org/10.1002/2014PA002636>.
- Rosenthal, Y., Boyle, E.A., Labeyrie, L., Oppo, D., 1995. Glacial enrichments of authigenic Cd and U in Subantarctic sediments: a climatic control on the elements' oceanic budget? *Paleoceanography* 10, 395–413. <https://doi.org/10.1029/95PA00310>.
- Saavedra-Pellitero, M., Baumann, K.H., Flores, J.A., Gersonne, R., 2014. Biogeographic distribution of living coccolithophores in the Pacific sector of the Southern Ocean. *Mar. Micropaleontol.* 109, 1–20. <https://doi.org/10.1016/j.marmicro.2014.03.003>.
- Schulz, M., Mudelsee, M., 2002. REDFIT: estimating red-noise spectra directly from unevenly spaced paleoclimatic time series. *Comput. Geosci.* 28, 421–426. [https://doi.org/10.1016/s0098-3004\(01\)00044-9](https://doi.org/10.1016/s0098-3004(01)00044-9).
- Shukla, S.K., Crosta, X., Ikebara, M., 2023. Synergic role of frontal migration and silicic acid concentration in driving diatom productivity in the Indian sector of the

- Southern Ocean over the past 350 ka. Mar. Micropaleontol. 181, 102245. <https://doi.org/10.1016/j.marmicro.2023.102245>.
- Sigman, D.M., Boyle, E.A., 2000. Glacial/interglacial variations in atmospheric carbon dioxide. Nature 407, 859–869. <https://doi.org/10.1038/35038000>.
- Sinha, B., Buitenhuis, E.T., Le Quéré, C., Anderson, T.R., 2010. Comparison of the emergent behavior of a complex ecosystem model in two ocean general circulation models. Prog. Oceanogr. 84, 204–224. <https://doi.org/10.1111/j.1365-2486.2005.1004.x>.
- Skinner, L.C., Fallon, S., Waelbroeck, C., Michel, E., Barker, S., 2010. Ventilation of the deep Southern Ocean and deglacial CO₂ rise. Science 328, 1147–1151. <https://doi.org/10.1126/science.1183627>.
- Studer, A.S., Sigman, D.M., Martínez-García, A., Benz, V., Winckler, G., Kuhn, G., Esper, O., Lamy, F., Jaccard, S.L., Wacker, L., Oleynik, S., Gersonde, R., Haug, G.H., 2015. Antarctic Zone nutrient conditions during the last two glacial cycles. Paleoceanography 30, 845–862. <https://doi.org/10.1002/2014PA002745>.
- Stuiver, M., Reimer, P.J., 1993. CALIB rev. 8. Radiocarbon 35, 215–230.
- Tamsitt, V., Drake, H.F., Morrison, A.K., Talley, L.D., Dufour, C.O., Gray, A.R., Griffies, S., Mazloff, M.R., Sarmiento, J.L., Wang, J., Weiher, W., 2017. Spiraling pathways of global deep waters to the surface of the Southern Ocean. Nat. Commun. 8, 172. <https://doi.org/10.1038/s41467-017-00197-0>.
- Tangunian, D., Berke, M.A., Cartagena-Sierra, A., Flores, J.A., Gruetzner, J., Jiménez-Espejo, F., LeVay, L.J., Baumann, K.H., Romero, O., Saavedra-Pellitero, M., Coenen, J.J., Starr, A., Hemming, S.R., Hall, I.R., 2021. Strong glacial-interglacial variability in upper ocean hydrodynamics, biogeochemistry, and productivity in the southern Indian Ocean. Comm. Earth & Environ. 2, 80 doi: 1038/s43247-021-00148-0.
- Thöle, L.M., Amsler, H.E., Moretti, S., Auderset, A., Gilgannon, J., Lippold, J., Vogel, H., Crosta, X., Mazaud, A., Michel, E., Martínez-García, A., Jaccard, S.L., 2019. Glacial-interglacial dust and export production records from the Southern Indian Ocean. Earth Planet. Sci. Lett. 525, 115716. <https://doi.org/10.1016/j.epsl.2019.115716>.
- Tréguer, P.J., 2014. The Southern Ocean silica cycle. Compt. Rendus Geosci. 346, 279–286. <https://doi.org/10.1016/j.crte.2014.07.003>.